Slip Validation and Prediction for Mars Exploration Rovers

Jeng Yen
Jet Propulsion Laboratory,
Pasadena, California, USA
jeng.yen@jpl.nasa.gov

Abstract

This paper presents a novel technique to validate and predict the rover slips on Martian surface for NASA's Mars Exploration Rovers. Different from the traditional approach, the proposed method uses the actual velocity profile of the wheels and the digital elevation map (DEM) from the stereo images of the terrain to formulate simplified equations of motion of the rovers. A weighted factor to the wheel-ground speed from the empirical data comprises the velocity equations of the simplified differential-algebraic system of the rover motion. Applying the discretization operator to these equations, the full kinematics state of the rover is then resolved by the configuration kinematics solution in the Robot Sequencing and Visualization Program (RSVP) [1,6,10]. This method produced accurate simulation of the rover movements compared with these of the earth testing vehicle. Using the telemetry from the onboard Visual Odometry [2], the simulated rover path also compares well with the actual track of the vehicle. Preliminary results indicated that the proposed computational method is very effective in planning the path of the rovers on the high-slope areas.

Keywords: MER, Mars Rover, multi-body simulation, configuration kinematics, autonomous navigation.

1 Introduction

In January 2004, NASA successfully landed two robot geologists : Spirit and Opportunity Mars Exploration Rovers (MER), on the surface of Mars. The mission's primary objective is to find evidence of past water on Gusev Crater and Meridiani Planum, two locations on the opposite sides of the planet. To date, after 20 kilometer accumulated distance of driving, they have succeded in the primary goal and are still roaming on the Martian surface for scientific targets. This tremendous acheivement owes to the ability of the on-board mobility and the ground sequence simulation for planning safe path for the rovers in the harsh Martian surface. We will address the MER vehicle simulation in this presentation.

Simulations of space-borne systems have been well-developed and successfully applied to many of the past and current NASA missions. The modeling and simulation of spacecraft has been carried out using multi-body system dynamics [4]. The design and operation of the spacecraft are based on the predicted behavior using high-fidelity simulation tools [5]. The modeling of robotic vehicles for the surface operation is, however, very different from those of traditional spacecraft operations. The most important aspect of the rover's model is the need to interact with the surrounding terrain. Based on the knowledge of the terrain, the simulator will predict the states of the rover. This requires effective modeling of the rover-terrain interaction. In addition, the multi-body rover model should include all the motorized mechanisms that are commandable for a comprehensive sequence simulation.

Robot Sequencing and Visualization Program (RSVP) provides the capability to operate and control the MER rovers. Typically, the rovers are commanded once per Martian day, called a sol. A sequence of commands sent in the morning specifies the sol's activities: what images and data to collect, how to position the robotic arm, or where to drive. At the end of each sol, the rovers send back the data and images human operators will use to plan the next sol's activities. Using the command-level editing and the sequence-level simulation of RSVP, the operators can select the next sol's mobility commands and visualize the predicted motion [6,8].

The sequence rehearsal tool in RSVP is based on modeling and simulation of the multi-body mechanical system [10]. The methodology has been developed to support a real-time interactive graphics mode for the visualization tool, using the configuration kinematics algorithm [3] and 3D terrain models. The sequence simulation is carried out using the on-board flight software modules for realistic rover behavior.

Determined by the solution of six wheel-terrain contact equations, the algorithm solves the vehicle's wheels, steering and suspension linkages, and the position and orientation of the chassis. It treats the underlying mathematical model as an inverse-kinematics problem, and carries out the solutions using the computational techniques for constrained optimization. In this framework, the objective functions are comprised of three conditions: the rover's internal differential mechanisms, the wheel-terrain contact, and the commanded rover location and heading as shown in [3].

During the surface mission phase, the configuration kinematics simulation has provided fast and high quality results for path planning on relatively level ground. The simulation results of the rover position and orientation using terrian DEM from the aquired images are remarkablely close to those of the on-board estimation [8]. But on steep hillsides, in mixed sand/rock terrains inside craters, and even when crossing sandy ripples in the otherwise flat plains of Meridiani, the simulation has not, as expected, been able to acurately predict the rover position due to large slips. The only on-board sensor that can detect position slip is the Visual Odometry (VisOdom) [2]. The VisOdom software compares two pairs of images to detect and track a set of features between these images. The motion of the features is used to update the vehicle's on-board position estimate according to the algorithm described in [9]. On high-slip areas, VisOdom can produce accurate onboard position estimates, and has become a critical component of rover's safety systems. The telemetry of these onboard positions will be used to validate the proposed slip model.

Conventional simulation of wheeled vehicles often uses a contact compliance formulation to deal with the complex wheel-terrain surface contact model [4]. The contact forces on the wheel are represented by a linear spring-damper actuator. Based on the penetrative distance between the terrain and the wheel, a force will be applied to the vehicle's equations of motion to generate the dynamical effects from the contact. However, the numerical solutions of this dynamical system suffers from instability and because the rough terrain profile and the physical limits of the linkages (e. g., the bumper-stops) can inject impulsive forces in such systems. All these modeling and numerical difficulties prevent a novel solution that achieves the real-time simulation of the rover traversal on a rocky terrain.

To overcome these difficulties a set of simplified dynamic equations is first developed, and then a heuristic wheel-ground speed estimation is applied to reduce the contact dynamics to a psuedo-dynamics for the slip model. This technique has been implemented in RSVP to compute ARC and TURN for MER vehicles. In the following section, we'll present the underlying framework of the MER vehicle simulation.

Figure 1: Mars Exploration Rover.

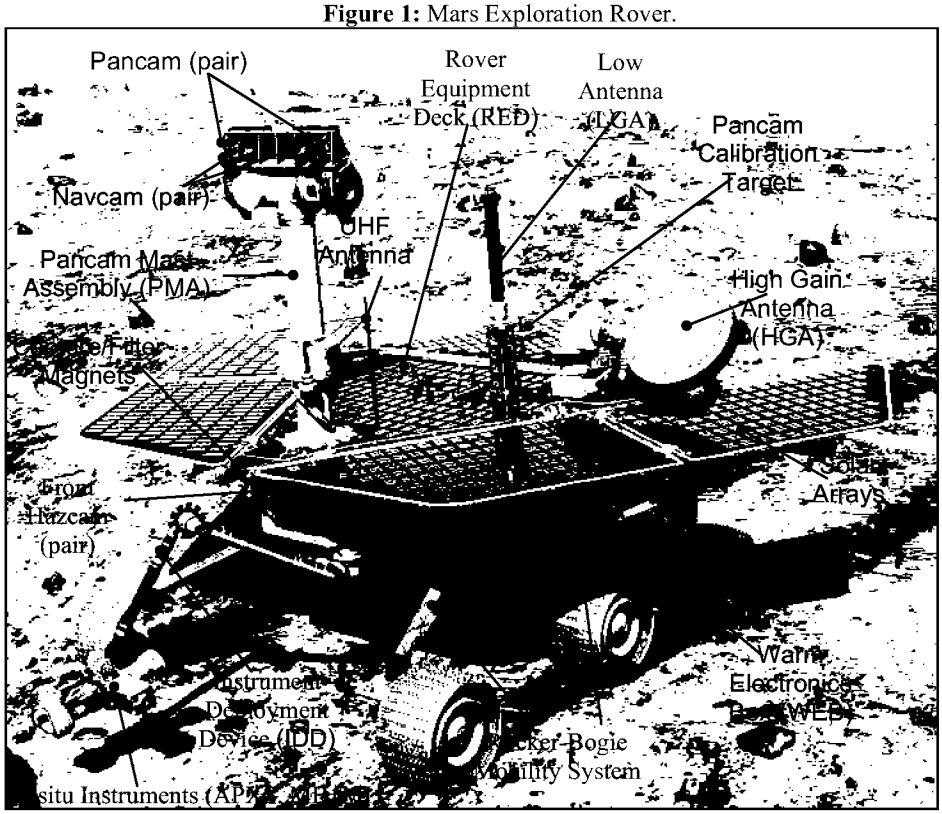

2 Mars Rovers Simulation

In RSVP, the MER vehicle model is represented by a set of hierarchical sub-graphs of the mechanism models for the primary motion systems. These sub-graphs are the foundation block for receiving sensed data, interpreting commands and predicting the physical states of the corresponding mechanical systems as shown in Fig. 1. The mobility mechanism consists of the Rocker-Bogey-Differential (RBD) suspension and the four-wheel steering systems. As shown in Figure 1, the suspension and the rover's kinematics, e.g., position and attitude, comprise a multi-body system of 10 states. These are the basic states of the rover's model for mobility.

Note that six wheels with four steering motors comprise additional states of the full vehicle system, but these acuators are fully cotrolled by the onboard mobility software. Thus, the steering and driving motors are not accounted for by the RSVP rover simulation model. In particular, the onboard mobility software controls the drive motors following a specific velocity profile to achieve Ackermann steering on flat ground [9].

2.1 Constrained Multi-body System

The equations of motion of multi-body dynamic systems can be written as

$$\begin{aligned} \ddot{q} &= M^{-1}[f - G^T\lambda] \\ g(q) &= 0 \end{aligned} \tag{1}$$

where q is the generalized state, $\dot{q}$ and $\ddot{q}$ are the velocity and acceleration of the generalized states, M is the generalized mass matrix, f is the applied force, g is the algebraic constraint and $G = \frac{d}{dq}g$ is the Jacobian of the contraint, and $G^T\lambda$ represents the constriant reaction force, where λ is the Lagrange multiplier. The generalized coordinates q of the MER vehicles consist of 10 states, the vehicle's position and orientation states, joint angles of the left and right rockers, and joint angles of the bogeys. The constraints g containts a linear equation of the differential, e.g., the joint angles of the left and right rockers are equal and of the opposite sign, and six rigid contact equations

$$g_{contact}(q) = dist(w,c) = 0$$

where the distance of the wheel center to the terrain is equal to the wheel radius. Thus, Eq. 1 represents a system of only three degrees of freedom.

The solution of Eq. 1 can be obtained using the standard methods for Differential-Algebraic Equations (DAE) [12], where a class of the discretization operators is directly applied to the differential part of Eq. 1. The stability of the solution in this approach often imposes a restricted step size of the discretization methods because of the so-called *artificial stiffness*. Alternatively, Eq. 1 can be rewritten to a state-space form, e.g., a set of differential equations representing the true degree of freedom in the system. One of these reduction techniques is the generalized coordinate partitioning method [4] which has been widely used in the simulation of ground vehicles in the automotive industry.

2.2 Coordinate Partitioning for Constrained Multi-body Dynamics

The state-space representation of the rover motion of (1) can be expressed as

$$\begin{aligned} \ddot{x} &= X^T M^{-1}[f - G^T\lambda] = f_x \\ \ddot{y} &= Y^T M^{-1}[f - G^T\lambda] = f_y \\ \ddot{\theta} &= \Omega^T M^{-1}[f - G^T\lambda] = \tau_z \end{aligned} \tag{2}$$

where $[x, y, \theta]$ are the rover x-coordinate, y-coordinate and heading , the projection operators are defined as $x = X^T q, y = Y^T q, \theta = \Omega^T q$. It is interesting to note that the closed form state-space representation of Eq. 2 for a general multi-body dynamical system can be very difficult to obtain. The right-hand-side of Eq. 2 is often evaluated using the full generalized acceleration in Eq. 1.

Applying the time integration operator to Eq. 2 yields the *independent coordinate* of q. Applying the solution of the independent coordinates, the *dependent coordinates* in q can be obtained by solving the constraint equations, e.g.,

$$\begin{aligned} x &= \int v_x dt = \iint f_x dt \\ y &= \int v_y dt = \iint f_y dt \\ \theta &= \int \omega_z dt = \iint \tau_z dt \\ g(q) &= 0 \end{aligned} \tag{3}$$

where $[v_x, v_y, \omega_z]$ is the velocity of the generalized coordinates $[x, y, \theta]$.

2.2.1 Configuration Kinematics

Apply directly the desired rover position from an ARC or a TURN command, Eq. 3 can be written as

$$\begin{aligned} x - x_{arc} &= 0 \\ y - y_{arc} &= 0 \\ \theta - \theta_{arc} &= 0 \\ g(q) &= 0 \end{aligned} \tag{4}$$

where $[x_{arc}, y_{arc}, \theta_{arc}]$ is the result of commended location and heading. The solution of Eq. 4 is then obtained by a Newton-type iterative method. Regular Newton-type iteration requires that g is *smooth* (e.g. $g \in C^2$ has 2nd order derivatives) to ensure a fast convergence. This prerequisite of a robust convergence is violated since the roughness of the terrain has been embedded in the contact equations. When the rocker or bogey linkages reach their limits, the abruptness of the iteration can induce unpredictable solutions of the configuration. To overcome these numerical difficulties, we apply a weight factor to the residual of each contact equation. During the iterations, the weight factor for a given wheel can be reduced to zero to relax the contact condition. Whenever the wheel leaves the ground, its corresponding weight factor is set to zero for a total relaxation of this wheel-terrain contact. The re-scaling of the weight factors is coupled with the global search algorithm, which can detect the joint limits associated with each wheel-terrain contacts, and can sample small perturbations around the contacting locations to determine the occurrence of a separation of the wheel and the ground.

The step-selection strategy used in the global search is a backtracking line search algorithm that monitors the progress of the iteration. For a smooth terrain profile, the iterative solution generated by the Newton method converges very rapidly to a local minimum of the nonlinear equations. However, the rate of convergence can be tremendously decreased when a non-smooth terrain profile appears. Special care is taken to maintain a robust and efficient solution in the case of a non-smooth terrain profile. Although the problem in hand is ill posed (i.e., it is well-known that the Newton method cannot treat non-smooth equations), we developed a heuristic solution to ease the computational difficulty in the iterations. In practice, the wheel-terrain contact is treated as a non-penetrative type, which is not a realistic portrait of the nature of the wheel-terrain interaction. Therefore, a search direction to the wheel-terrain contact may not be in-line with the normal direction of the terrain (at the contact location), instead; it could be anywhere along the perimeter of the wheel. The heuristic leads to modeling the wheel-terrain contact equation as the distance constraint between the wheel center and the terrain profile. On level ground, the solution of Eq. 3 by the aforemention techniques results in an efficient and accurate estimation of the commanded location of the MER vehicles [6,10].

2.2.2 Estimation of Independent Velocity

Equation 3 can be again re-written as a first-order differential-algebraic equations by applying the time differentiation operator to the state variables $[x, y, \theta]$ of Eq. 4. This yields

$$\begin{aligned} \dot{x} - v_x &= 0 \\ \dot{y} - v_y &= 0 \\ \dot{\theta} - \omega_z &= 0 \\ g(q) &= 0 \end{aligned} \qquad (5).$$

In fact, Eq. 5 can also be obtain from Eq. 4 if we declare that the time derivatives are

$$v_x = \frac{d}{dt} x_{arc},\ v_y = \frac{d}{dt} y_{arc}, \text{ and } \omega_z = \frac{d}{dt} \theta_{arc}.$$

The vehicle's speed when performing ARCs and TURNs has been measured in the earth-testbed, so these empirical vehicle speed profiles/tables may be used directly in Eq. 5. A straightforward calculation leads to the "slip tables" approach which use only the empirical data to approximate the slips. Then the modified Eq. 3 is resolved for the add-on slips. However, only the gross motion can be represented by these tables, and the dimension of these tables can be very large.

Using rigid-body motion, the velocity of the independent states can be obtained from a consistent wheel-ground speed. Since the onboard drive motor controller is always keeping up with a pre-defined profile, we can use the speed profile and the local terrain geometry for an approximated velocity of the independent variables. Moreover, the wheel-terrain slip can be incorporated in this approximation so that the vehicle total slip can be computed accordingly. A heuristic approach is to "avarage" the wheel-ground speed of each wheel for the independent velocity $[v_x, v_y, \omega_z]$. Let the $i-th$ wheel's velocity projected onto the plane interpolation of the terrain patch under the wheel be

$$v_i^W = (I - P_i P_i^T)\bar{v}_i^W \qquad (6)$$

where $(I - P_i P_i^T)$ is the projection and $\bar{v}_i^W$ is the nominal wheel speed. Assuming the rigid contact condition, the wheel-ground speed is along the tangential direction of the contact plane, as shown in Eq. 6. For all six wheels in contact with ground, the rover velocity is a linear combination of the wheel-ground velocity, e.g., vehicle's velocity is within the convex hull of all the wheel velocity. Apply the partitioning operator and a weight factor to each of the driving wheels yields

$$\begin{aligned} v_x &= X^T \sum_i \alpha_i v_i^W + d_x \\ v_y &= Y^T \sum_i \alpha_i v_i^W + d_y \\ \omega_z &= \Omega^T \sum_i \beta_i (r_i \times v_i^W) \end{aligned} \qquad (7)$$

where α_i and β_i represent the weight factors, and r_i is the location of the wheel in the rover's navigation

frame, and (d_x, d_y) is the sliding vector of the rover. Typically, the sliding vector is along the down slope direction on a local patch of the terrain where the vehicle is treated as a point-mass on a gravitational field, e.g.,

$$d_x = \iint_t f_x^g dt$$

$$d_y = \iint_t f_y^g dt$$

where f_x^g and f_y^g are the gravitational forces acting on the independent coordinates (x, y), respectively. Using Eqs. 5 and 7, the rover position and orientation, and the joint angles of the rockers and bogeys can be obtained. The weight factor is selected based on the local geometry, e.g., the *wheel-ground angle*. The magnitude of sliding vector is determined by the experimental data of the slip tables. Since the maximum tilt of the static stable configuration of the MER vehicles is 35 degrees, the weight factor and sliding factor are obtained from the results interpolated between 0 to 30 degrees.

3 Numerical Examples

The numerical test for the rover slip model is illustrated on the Figs. 2-5. The rover started on a flat surface with 14 degrees slope at the origin (0,0). The testing sequence comprised of a 3-meter ARC driving downhill, then a 3-meter ARC back up to the origin, then TURN to 0 degree heading, then driving back and forth with two 3-meter ARCs. Comparing the "no slip" simulation using Eq. 4, indicated by the solid rover in the Figs., with the simulation using Eq. 5 and 7, indicated by the watermarked rover, the slippage predicted by the simulation matches well with those of the experiments. When driving in the downhill direction, Fig.1 shows a 14% down-slope slip of the straight arc. The uphill straight arc illustrated in Fig. 2 shows a similar down-slope slide. After a turn to line up to a side slope direction, the forward and back arcs slide toward the down-slope direction at about 10 % of the traveling distance,

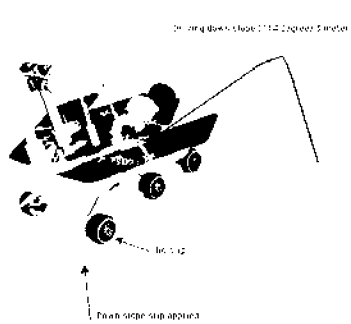

Figure 2 Down Slope Driving 14% Slip

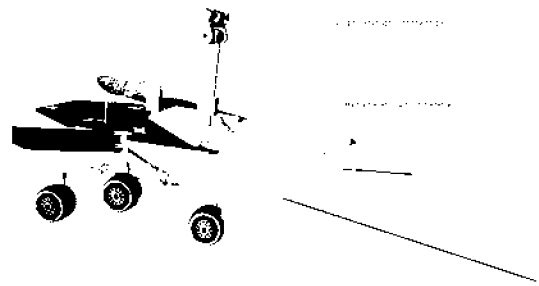

Figure 3 Up Slope Driving 14-16% Slip

Figure 4 Side Slope Driving 10% Slip

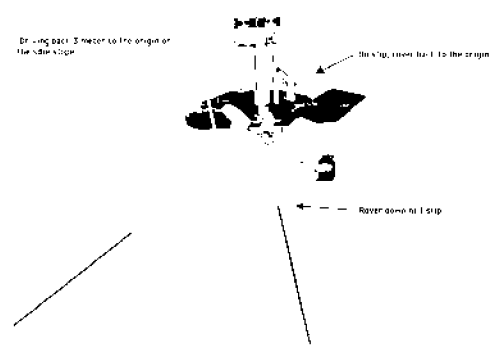

Figure 5 Side Slope Driving 10% Slip

We learned during our initial drives in each terrain that driving on level ground typically leads to accurate and predictable mobility performance; e.g., Spirit only accumulated 3% position error over 2 kilometers of driving [8]. Before driving into Endurance Crater, a series of driving tests were carried out to establish a set of slip tables for the MER vehicles. These tables measure the slippage percentage based on the tilt angle of the vehicle assuming a flat surface underneath. We have implemented the slip tables in RSVP simulation as the baseline method to compute the weight factors in Eq. 7. From the test results, the vehicle exhibits about 1% slip (of the total driving distance) per degree on a slope ranging 10-20 degrees

sandy surface. Similar performance is seen on the MER vehicles when driving on the Martian surface covered with "blue berries", which are small round pebbles.

3.1 High Slope Hillside

While most of the distance covered by the rovers was on level ground, most of the sols and most of the approach drives occurred on slopes. The rovers invariably slip when driving on slopes, making VisOdom essential for safe and accurate driving. To construct a successful drive on high slope areas, accurate estimation of the commanded location can only be obtained with the correct vehicle slips.

On sol 1211, Opportunity drove toward the rim of Victoria crater to take images of Cape St. Mary. The vehicle was on a modest terrain of 7-10 degree slope tilted left as shown in Fig. 6, but the drive would take the vehicle very close to the edge of the Crater (about 2 meters from the visible rim side), making the drive nerve-racking. We took the vehicle 4 meters forward and pointed the camera to Cape St. Mary 100 degrees left and 70 meter away.

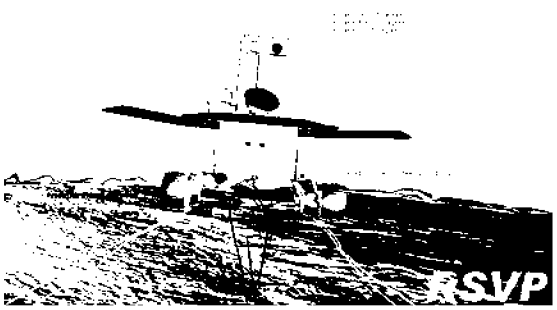

Figure 6 Approach to Victoria Rim with 5% Slip

Three rover paths in the blue lines are shown in Fig. 6, where the left one is the obtained by the CK method, the right line is the prediction of proposed method. The Onboard Visodom correction of the rover location is the blue line in the middle. Note that the 5% slips along the right side of the slope matched well with the VisOdom data.

4 Acknowledgements

Thanks to Jeff Biesiadecki for insightful discussion on the motor controller onboard the MER flight system, RSVP team lead Brian Cooper and the team members (Frank Hartman, Scott Maxwell, and John Wright) for supporting the inclusion of the slip model in RSVP, Mark Maimone for fruitful discussion on validatiing the slip model using the telemetry and VisOdom data.

The work described in this paper was carried out at the Jet Propulsion Laboratory, California Institute of Technology, under a contract to the National Aeronautics and Space Administration.

References

[1] B. Cooper, F. Hartman, S. Maxwell, and J. Wright, J. Yen. "Using RSVP for Analysing State and Previous Activities for the Mars Exploration Rovers." In *SpaceOps*, Montreal, Canada, 2004.

[2] Yang Cheng, Mark Maimone, and Larry Matthies. "Visual odometry on the Mars Exploration Rovers." In *IEEE Conference on Systems, Man and Cybernetics*, The Big Island, Hawaii, USA, October 2005.

[3] J. Yen, A. Jain and B. Balaram, "ROAMS: Rover Analysis, Modeling and Simulation," in the proc. Of 5th iSAIRAS, ESA, Netherland, 1999.

[4] E. J. Haug, "Computer Aided Kinematics and Dynamics of Mechanical Systems", Allyn-Bacon, 1989.

[5] Biesiadecki, J., Henriquez, D., and Jain, A., "A Reusable, Real-Time Spacecraft Dynamics Simulator," *Proceedings of the Sixth Digital Avionics Systems Conference*, Irvine, CA, October 1997.

[6] S. Maxwell, B. Cooper, F. Hartman, J. Wright, J. Yen, and C. Leger, "The best of both worlds: Integrating textual and visual command interfaces for mars rover operations," in *Proc. IEEE Syst., Man, Cybern. Conf.*, 2005, vol. 2, pp. 1384–1388.

[7] Rongxing Li, Brent A. Archinal, Raymond E. Arvidson, Jim Bell, Philip Christensen, Larry Crumpler, David J. Des Marais, Kaichang Di, Tom Duxbury, Matt Golombek, John Grant, Ronald Greeley, Joe Guinn, Andrew Johnson, Randolph L. Kirk, Mark Maimone, Larry H. Matthies, Mike Malin, Tim Parker, Mike Sims, Shane Thompson, Steven W. Squyres, and Larry A. Soderblom. Spirit rover localization and topographic mapping at the landing site of Gusev Crater, Mars. JGR-Planets, Special Issue on Spirit Rover, 111(E02S06, doi: 10.1029/2005JE002483). http://www.agu.org/journals/ss/SPIRIT1/.

[8] Mishkin, A.H.; Limonadi, D.; Laubach, S.L.; Bass, D.S.; "Working the Martian night shift - the MER surface operations process," Robotics & Automation Magazine, IEEE Volume 13, Issue 2, June 2006 Page(s):46 – 53.

[9] Biesiadecki, J. J., Leger, P. C., and Maimone, M. W. (2007). Tradeoffs between directed and autonomous driving on the Mars Exploration Rovers. International Journal of Robotics Research, 26(1):91–104.

[10] J. Yen, B. Cooper, F. Hartman, S. Maxwell, and J. Wright. Sequence rehearsal and validation on surface operations of the Mars Exploration Rovers. In *SpaceOps*, Montreal, Canada, 2004.
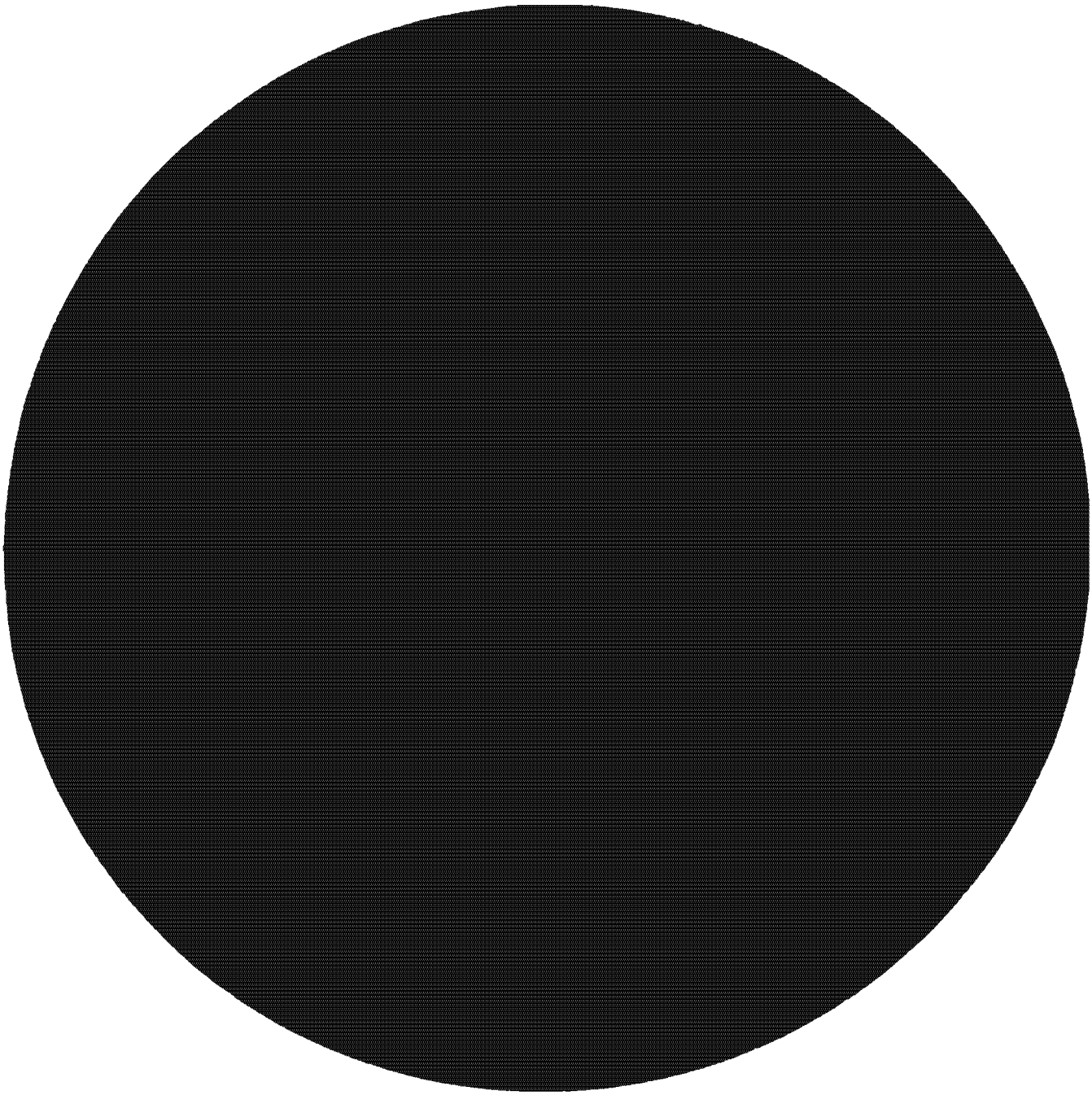
End of File